CHAPTER 12

CONVECTIVE-HEATING MEASUREMENTS

by

Gary T. Chapman, Layton Yee,
Dale L. Compton, and Max E. Wilkins

NASA-Ames Research Center

CONVECTIVE-HEATING MEASUREMENTS

Gary T. Chapman, Layton Yee,
Dale L. Compton, and Max E. Wilkins

12.1 INTRODUCTION

Ballistic ranges and free-flight tunnels have only infrequently been used to measure convective heating because of the difficulty of determining the rate of temperature rise of the model surface in flight. Although considerable effort has been made to develop miniature active telemetry systems for this purpose, the lack of data obtained shows the difficulty of this approach. A brief description is given of what has been done and what the future holds in store for active telemetry. However, three methods of determining heat-transfer rates have been developed to the level of producing reportable data in the last 15 years for use in ballistic ranges; one is based on passive telemetry, while the other two are completely different in approach. Other convective heating data have been deduced from studies of recovered ablated models. These techniques will be summarized in this chapter.

The passive telemetry system[12.1] uses the electromagnetic coupling between two coils, an energized (signal) coil in the model which flies through a fixed coil (antenna) in the ballistic range. The coil in the model is energized by the output of a thermocouple, and in turn induces a current in the pickup coil in the range. The pickup coil output is proportional to the current from the thermocouple and hence to the surface-temperature rise. By firing the model through a series of coils placed along boresight a temperature-time history of the model is obtained and from this the heat transfer can be inferred.

The second method involves calorimetric measurement of the total aerodynamic heat in the recovered model, immediately after it has been decelerated from a high initial velocity by aerodynamic drag[12.2]. Since the heat content of the recovered model is accurately measured in a calorimeter, a series of tests at various launch velocities can be analyzed to yield heat-transfer rates. One of the limitations of this method is that, if the heating rate to the model becomes high enough (e.g., by increasing launch velocity) the model will begin to melt and lose material so that the calorimeter will fail to measure the total heat input. This particular limitation becomes the basis for the third method.

The third method is based on the detection of the time of onset of melting of the model[12.2]. The onset of melting on free-flight models can be fairly reliably detected, since the molten material runoff apparently forms a fine opaque mist which yields a shadow image in the range photographs. Surface melting on the model ordinarily occurs first where the heating rate is highest – at the stagnation point for most models. The time at which melting first occurs is a measure of the stagnation-point heating rate.

These three methods are basically independent of each other and each has inherent advantages and disadvantages. It should be noted that all three are applicable with most guns and ballistic facilities. Each places its own set of requirements on range size, pressure levels, and auxiliary equipment.

12.2 ACTIVE TELEMETRY

Considerable effort has been expended (notably, M. Letarte et al., of Canadian Armament Research and Development Establishment, and P.L. Clemens et al., of von Kármán Gas Dynamics Facility, ARO, Inc.) on active telemetry systems to measure heat-transfer rates. The telemeters used are typically transistorized FM-FM systems with a carrier frequency of about 60 MHz, and a subcarrier frequency of about 50 KHz. Thin-film gages have been the most frequently used temperature sensor for these systems.

The development of an active telemetry system for high-velocity launches has been hampered by the fragility of the electronic components built into the models. Transistors, for instance, are unusable in their off-the-shelf state and must be carefully potted. With careful selection of suitable components and tedious manufacture, active telemetry models have been tested successfully. The acceleration loads have been limited to about 200,000 g (quite modest by light-gas-gun standards), which resulted in launch velocities of less than 3 km/sec. The use of integrated circuits might overcome many difficulties of the past; unfortunately, however, there is evidence that above 4 km/sec the ionized sheath around the model will impair the data transmission in the case of blunt-nosed models.

Clemens has compiled a comprehensive bibliography on telemetry suitable for ballistic-range use[12.3]. His survey listed 30 references chronologically from June 1954 to July 1962, including the extensive work of Letarte.

12.3 PASSIVE TELEMETRY

The models used in passive-telemetry heat-transfer tests contain a copper-constantan thermocouple, the active element, connected in series with a low-resistance coil, as shown in Figures 3.31 and 12.1. The hot junction, located at the nose of the model in Figure 12.1, is formed by the copper-calorimeter nose cap and the constantan wire core, which also joins a copper disk buried in the model (the cold junction). The small copper coil, wound on an insulating form, joins the disk to the edge of the calorimeter.

The detector is a multi-turn, single-layer, center-tapped, coil wound on a cylindrical dielectric form and enclosed by an electrostatic shield to minimize spurious signals caused by the model's static charge, its ionized flow field, and wake. A photograph of a pickup coil with its shield and support is shown in Figure 12.2.

The experimental setup shown in Figure 12.3 illustrates one of several identical detector stations. The magnetic field caused by current flow in the small coil in the model induces an e.m.f. on the pickup coil. This signal, recorded on a differential-input oscilloscope, is proportional to the current flowing in the excited coil and to the rate of change of mutual inductance between the two coils. Since all these parameters are either known before the flight or are measured during the flight of the model, the temperature history of the calorimeter can be determined. A representative signal is shown in Figure 12.4. Only the central feature (i.e., the antisymmetric rise, fall, and return to zero) is of importance. The other signals are electromagnetic interference picked up from the firing of sparks in the shadowgraph stations.

12.3.1 Analysis

The voltage induced in the pickup coil by the moving model is given by Faraday's law

$$e = -10^{-6}\frac{d(MI)}{dt} , \tag{12.1}$$

where

e = e.m.f. induced in the pickup coil, volt

M = mutual inductance between the coils, μH

I = current flowing in the model coil, A.

If the current is assumed to be constant during the short passage time in the coil, the voltage induced in the pickup coil is

$$e = -10^{-6} I \frac{dM}{dt} . \tag{12.2}$$

The mutual inductance between the two coils may be expressed[12.4] as

$$M = 0.00986 \frac{a^2 N_a N_A}{b}\left(\frac{x+b}{\sqrt{[(x+b)^2 + A^2]}} - \frac{x-b}{\sqrt{[(x-b)^2 + A^2]}}\right), \tag{12.3}$$

where

a = radius of model coil, cm

A = radius of pickup coil, cm

$2b$ = length of pickup coil, cm

N_a = number of turns of model coil

N_A = number of turns of pickup coil

x = axial distance between the centers of the coils, cm.

With the appropriate coil dimensions substitued into Equation (12.3), M is defined. Equation (12.3) may then be differentiated with respect to x, and this derivative substituted into Equation (12.2) (after transforming Equation (12.2) from time to distance as an independent variable by $dM/dt = V dM/dx$) to give

$$e = -8.826 \times 10^{-6}\, IV \left\{[(x+1.905)^2 + 25.806]^{-3/2} - [(x-1.905)^2 + 25.806]^{-3/2}\right\} . \tag{12.4}$$

In order to reduce the data from the peak voltage recorded on the oscilloscope, Equation (12.4) is differentiated to find the value of x for which e is maximum. The substitution of this value of x into Equation (12.4) yields

$$e_{max} = kIV , \tag{12.5}$$

where, for the particular coil dimensions of Reference 12.1, $k = 3.78 \times 10^{-8}$ volt sec/ampere cm. The value of e_{max} can be determined from the oscilloscope record; V (cm/sec) can be calculated from the time distance

history recorded in shadowgraphs and on electronic timers. Thus, I, the current flowing through the model coil, can be determined. The product of I and the known circuit resistance of the model gives the voltage output of the thermocouple. The temperature rise of the nose cap can then be obtained from a copper-constantan thermocouple calibration curve.

The preceding calculations are valid only when the model axis and pickup coil axis coincide. For off-center shots, the voltage induced in the coil is still given by Equation (12.2); however, the expression for M (Eqn(12.3)) must be modified to account for the radial distance between the axes of the two coils. This expression has been evaluated on a digital computer[12.1]. The result of this evaluation, as applied to the coils in that reference, is shown in Figure 12.5 as a correction-factor plot. This curve was verified experimentally by measuring the mutual induction (using a probe coil with a measured current to simulate the model coil in off-center positions), as shown by the experimental points.

The raw experimental data give a temperature-time history of the inner surface of the copper-cap calorimeter. To compute the heat-transfer rate at the stagnation point, the following assumptions are made:

(a) Temperature is uniform across the thickness of the copper cap.

(b) Conduction along the cap may be neglected.

(c) Conduction past the inner surface of the copper cap may be neglected.

The heat-transfer rate, $\dot{q}$, is obtained from the measured rate of rise of model surface temperature through the expression

$$\dot{q} = \frac{k l}{\alpha} \frac{dT}{dt}, \tag{12.6}$$

where

α = thermal diffusivity of copper

k = thermal conductivity of copper

l = thickness of the nose cap

T = measured temperature.

Assumption (a) is intimately related to the finite response time of the copper calorimeter cap. It has been shown[12.1] that the error incurred in making this assumption is less than 2 percent. Assumption (b) is satisfied because the heat-transfer rate over the entire front surface of the copper cap does not vary by more than 5 percent. Assumption (c) is fulfilled because the boron nitride behind the copper cap is a good heat insulator; the constantan stem is not only small but a relatively poor heat conductor (conductivity about 1/20 of that of copper) as well.

12.3.2 Design Factors

The working equations which define the signals to be expected indicate the significant parameters for designing the models and antennas, and selecting test conditions. Because the expected signals are small (less than 10 mV), it is important to optimize the design of the model and the antenna to obtain a favorable signal-to-noise ratio.

From Equations (12.2) and (12.3), the signal is proportional to the current in the model coil, the number of turns, and the square of its radius. The maximum allowable coil radius is fixed by the model size; and the maximum ampere-turns is obtained when the coil resistance is one-half that of the thermocouple. The constantan wire which forms the hot junction largely determines the circuit resistance. However, this wire must necessarily be small to minimize heat conduction away from the calorimeter, even though a larger wire would increase the signal potential of the model and facilitate its fabrication.

The coil form in the model must be a good insulator, and it must not deform when heat is applied to the nose cap to silver-solder the hot junction and the coil. Boron nitride, while not a strong structural material, fulfilled the requirements adequately when supported by an aluminum alloy afterbody.

The circuit resistance was accurately measured with a Wheatstone bridge before final assembly. Epoxy cement was used to join all nonelectrical surfaces and fill all voids.

To achieve efficient coupling with the model coil, the pickup coil should have a large number of turns and a small radius, as indicated by Equation (12.3). In practice, however, the number of turns is limited by the corresponding increase in the amount of noise picked up by a more sensitive coil. Moreover, it is desirable for the coil to have a high resonant frequency to insure flat response, which also limits the number of turns of the coil. The coil should be critically damped with a resistor whose value can be determined experimentally.

The size of the pickup coil is determined by the dispersion of the gun-launched models; that is, a coil too small would not only be more susceptible to damage from erratic launches, but the correction for off-center flights would be more critical. With the radius of the pickup coil four times the usual dispersion at the last coil station of successful launches, the off-center correction was found to be usually less than 10 percent.

12.3.3 Comparison With Other Techniques

The accuracy of the heat-transfer measurements using this technique is believed to be comparable to that made using calorimeter heat-transfer gages in shock tubes. (Some experimental data are shown in Figure 12.15.) Since the radiated field is essentially d.c., it is unaffected by the ionized sheath around the model, so that the technique is usable at hypersonic speeds. The hot thermocouple junction can be located in areas other than the stagnation region, e.g., on the afterbody, where this technique would have a distinct advantage over conventional wind-tunnel tests because of the absence of sting effects. On the debit side, the models are fragile, difficult to manufacture, and difficult to launch at high speeds. The vulnerability of the pickup coils to damage from model impacts is also an expensive nuisance.

12.4 CATCHER-CALORIMETER TECHNIQUE

The heat content of ballistic-range models can be determined by capturing them in a calorimeter after flight[12.2,12.6]. The test arrangement for this catcher-calorimeter technique is shown schematically in Figure 12.6. The model, held in a completely enclosing sabot, on being launched from the gun emerges from the sabot and enters the range, where it is photographed in spark-shadowgraph stations while decelerating. The model scale, model material, air density, and range length are selected so that the model slows below a speed of about a hundred meters per second before entering a catcher. The model decelerates to zero-forward velocity by piercing many sheets of paper and then falls through a funnel into the calorimeter, where its total heat content is measured.

As the model decelerates during its flight, a major portion of its kinetic energy is converted to heat in the surrounding air by virtue of the strong bow shock wave; some of the energy is delivered to the model surface by boundary-layer convection. The rates of energy loss and model heating are highly variable along the trajectory, and the analysis must allow for this.

12.4.1 Heat-Input Analysis

The instantaneous average heating rate over the model surface, $\dot{q}_{av}$, is defined as

$$\dot{q}_{av} = \frac{1}{A_w}\int_{A_w} \dot{q}_l' \, dA_w , \tag{12.7}$$

where $\dot{q}_l$ is the local heat-transfer rate, and A_w is the wetted area of the body. The functional relationship between $\dot{q}_{av}$, free-stream density, model scale, and velocity, for laminar flow, is taken as[12.5]

$$\dot{q}_{av} = K\left(\frac{\rho_\infty}{r}\right)^{\frac{1}{2}} V^n , \tag{12.8}$$

where ρ_∞ is the free-stream density, r is a reference length (e.g., radius of curvature at the stagnation point), V is the flight speed, and K and n are constants to be determined.

The total aerodynamic heat transfer to a model during a given trajectory can be expressed as

$$Q_{aero} = A_w\int_0^t \dot{q}_{av} \, dt' , \tag{12.9}$$

where t is the time of flight.

The equation relating velocity and time is

$$\frac{dV}{dt} = -\rho_\infty C_D A \frac{V^2}{2m} ,$$

where

m = model mass

A = reference area

C_D = drag coefficient,

This equation may be used to write Equation (12.9) in terms of V as the independent variable.

Then, from Equations (12.8) and (12.9), we obtain

$$Q_{aero} = \frac{-K2mA_w}{A(\delta_\infty r)^{\frac{1}{2}}}\int_{V_L}^{V_{catch}} \frac{V^{n-2}}{C_D} \, dV . \tag{12.10}$$

Since the velocity history and drag coefficient are known, evaluation of Q_{aero} depends only on a selection of n and K. The procedure for selecting n and K, to obtain a best fit to the experimental data, is normally

a least-squares procedure using differential corrections. For the case of constant drag coefficient Equation (12.10) has the simple form

$$Q_{aero} = \frac{K2mA_w}{AC_D(n-1)(\delta_\infty r)^{\frac{1}{2}}} \left(V_L^{n-1} - V_{catch}^{n-1}\right) . \tag{12.11}$$

12.4.2 Design Factors and Equipment

The design of tests which employ this technique requires that the model scale and material, range length, and ambient density be selected to slow the model to a suitable recovery speed by the time it reaches the catcher. This can readily be done by use of the equation which gives the velocity variation with distance flown for constant drag coefficient, which is

$$\frac{V}{V_L} = \exp\left[-\frac{\rho_\infty A}{2m} C_D x\right] . \tag{12.12}$$

This equation is plotted to show the velocity variation with the dimensionless distance $(\rho_\infty AC_D/2m)x$ in Figure 12.7. Similarly, in Equation (12.8), $\dot{q}_{av}$, and in Equation (12.9), Q_{aero}, are functions of velocity only, other test conditions being given. Hence they may be universally plotted against the dimensionless distance. Thus $\dot{q}_{av}$ has been given in Figure 12.7 in ratio to its value at launch and Q_{aero} in ratio to Q_{aero} at the catcher, which makes it unnecessary to specify K. The exponent n, however, has, for illustrative purposes, been assigned the value 3.15 (Ref.12.5). This figure may be used for the case of a constant drag coefficient and a heating rate which is dependent on the velocity to the 3.15 power, to design a total-heat-transfer experiment for any particular combination of model, test conditions, and ballistic-facility. For example, a 0.635-cm-diameter aluminum hemisphere at 1 atm ($C_D = 0.9$ and $\rho_\infty A/2m = 0.1$ meter^{-1}) takes on 95 percent of the heat and loses 78 percent of its velocity in 16 meters of flight. It can be seen from this figure that the major portion of the heating occurs when the velocity is still relatively high, a result of the near-cubic dependence of heating rate on velocity.

Calculations must also be performed to determine that the model does not begin to melt, since heat would then be discarded in the melted and vaporized material and would not all be found in the model at recovery. This requirement does not hold, however, if one wishes to study the heat that is absorbed by the remaining part of an ablated model.

12.4.2.1 Sabot Design

The sabot, in addition to its usual functions of supporting the model during the launch and providing a seal between model and launch barrel, also must be designed to minimize heating to the model from three unwanted sources: (1) barrel friction, (2) the compressed gas in front of the sabot, and (3) the hot propellant gas behind the sabot. The protection provided by a conventional split sabot alone against the driver gas has been found to be inadequate; the propellant gases can pass along the parting planes of the split sabot and scorch the model. This leakage can be largely prevented by a thin disk gas seal behind the sabot (see Section 3.4.1.1). The total enclosure of the model within the sabot and the evacuation of the launch barrel will control or eliminate heating from gas in front of the model. With plastic sabots, barrel friction is small and the heat generated at the barrel wall and conducted to the model is negligible during the very brief acceleration stroke. Hence, with suitable design, spurious heat inputs in the gun can be made small compared to Q_{aero}.

12.4.2.2 Catcher and Funnel

The catcher is designed to stop models flying at subsonic speed, intact and without appreciably altering their total heat content. A suitable catcher developed in the study reported in Reference 12.6 consists of many (50-100) sheets of building paper hung on a rack. Sheets are spaced so that the model will fall freely between any two sheets into the funnel.

The funnel is formed of wrapping paper with steep sides to minimize transit time. Squaring the corners reduced the tendency of the model to spiral down the funnel, because spiraling increases the descent interval and hence permits additional heat loss from the model to the funnel and the air.

12.4.2.3 Calorimeter Description and Analysis

A very sensitive type of calorimeter is required, since the heat deposited by a small model may be of the order of a joule (0.001 Btu). One type possessing the desired sensitivity and accuracy is the conduction calorimeter in which the temperature difference across a known thermal conductance is measured as a function of time for as long a time period as any sensible temperature difference exists. Such a calorimeter is shown schematically in Figure 12.8. The differential equation for the conductive heat transfer from the source to the isothermal sink (of large heat capacity) is

$$\frac{dQ}{dt} = K_1[T_A(t) - T_B] . \tag{12.13}$$

Thus

$$Q = \Delta Q = K_1 \int_0^\infty [T_A(t) - T_B]\, dt . \tag{12.14}$$

In practice a finite integration limit can replace the infinite limit on the integral in Equation (12.14). If properly selected, this finite truncation has a negligible effect on the results.

In the technique described here, the calorimeter consists of a thin cup into which the model drops, a heat sink to absorb the heat, and a controlled conduction path between the cup and heat sink. Figure 12.9 is a quarter-sectional view of such a calorimeter. To obtain a large value of $T_A(t)$ with a small heat input, it is important to keep the heat capacity of the cup very low. To obtain rapidly a spatially uniform equilibrium temperature with the hot model, a high thermal diffusivity is required in the cup material. A small thin silver cup meets these requirements. The cup is instrumented with several thermocouples on the bottom exterior. All but one of these are connected in series with the reference junctions located in the heat sink. The remaining thermocouple is used to determine absolute temperatures.

The heat sink is constructed of two large blocks of phosphor bronze. The silver cup is suspended in a cavity in the lower block. The purpose of two large blocks is to provide sufficient heat capacity that the temperature level T_B in Equation (12.13) does not change more than a few thousandths of a degree while temperatures are being recorded. Buried in the lower portion of the lower block are several iron-constantan thermocouples which utilized the heat sink as a constant temperature reference mass; all but one of these are the reference junctions for the cup thermopile, and the remaining one is used to record absolute temperature. The model enters the cup through a conical hole in the upper block. This hole is lined with a low conductivity material to minimize any heat transfer due to contact with the model as it drops through to the cup.

The conduction path between the cup and heat sink consists of small support arms made of low-conductivity material, such as epoxy resins. These are fastened between the cup and the rim of the cavity. The conductivity of these supports (proportional to the value of K_1 in Equation (12.13)) is made such that the major portion of the heat from the hot model is transferred to the heat sink in a few minutes. It is necessary to use very fine thermocouples on the cup to minimize both their heat capacity and their conductivity between the cup and the heat sink. The excess volume of the cavity can be filled with foamed plastic to minimize free convection.

The output of the thermopile is proportional to the instantaneous temperature difference $T_A(t)-T_B$. This output, in millivolts, is recorded on a strip chart recorder (or other suitable device) from which portions of a typical trace are shown in Figure 12.10. The integral under this temperature difference – time curve is proportional to the heat transfer. Measurements of heat inputs as low as 10^{-2} joule were found to be possible with such equipment[12.6]. The development of this highly sensitive and accurate calorimeter made this test technique possible since, as noted, heat quantities to be measured may range down to a joule.

To calibrate the calorimeter, preheated models are dropped into it to determine the constant K_1 in Equation (12.14) and to determine the effects of several variables on K_1 such as model geometry, model orientation in cup, model material, and nonuniform temperatures in the model, etc. The value of K_1 was found to be insensitive to these variables.

12.4.3 Reduction of Total-Heat-Transfer Data

The reduction of the total heat-transfer data proceeds from an energy balance. The thermal energy, Q, added to the calorimeter by the model is obtained directly from the area under the temperature versus time curve of the calorimeter and the calibration constant K_1. This increment of energy consists of two parts, the energy due to aerodynamic heating, Q_{aero}, and the energy due to possible temperature differences between the model and the calorimeter prior to launching the model. The increment in energy, ΔQ, can be expressed as

$$\Delta Q = Q_{aero} + mc(T_{Mi} - T_{Ai}) , \tag{12.15}$$

where m is the mass of the model, c is the specific heat of the model material, and T_{Mi} and T_{Ai} are the prelaunch model and calorimeter temperatures, respectively. Equation (12.15) may be solved for Q_{aero}. It is assumed that there are no extraneous heat sources. This assumption is justified if proper precautions are taken. (See Section 12.4.5 for the details of these precautions.) The initial model temperature is evaluated from the gun temperature prior to launch. To assure that the model attains the gun temperature, it is loaded as much as an hour prior to launch.

12.4.4 Typical Results

Some typical total heat-transfer data obtained with such a calorimeter technique are shown in Figure 12.11, where total aerodynamic heat input, Q_{aero}, is plotted as a function of launch velocity V_L for eight independent tests. These results are for a 0.635-cm-diameter aluminum hemisphere tested at 1 atm free-stream pressure. These data were analyzed to obtain the constant and exponent in the heat transfer Equation (12.8) by fitting Equation (12.11) to the data. From this, the instantaneous heat-transfer rates averaged over the wetted surface area may be plotted against velocity as in Figure 12.12. The experimental curve (solid line) is compared with a theoretical curve (dashed line) obtained using the stagnation-point results of Reference 12.7, together with the distributions of Reference 12.8, for the case of zero base heat transfer. It can be seen that the agreement is good.

12.4.5 Error Analysis

The accuracy of the total heat-transfer measurements depends primarily upon the accuracy of the calorimeter measurements and the size of extraneous heat sources and sinks. The calorimeter precision can be determined from

calibration by examining sensitivity and repeatability. The extraneous sources of heating to be considered are:

1. Heating from gases in front of the model while the model is traversing the launch tube.
2. Heating caused by propellant gas leaking through the sabot to the model.
3. Heat loss due to long subsonic flight.
4. Heating and/or cooling during capture in the catcher and funnel.

As noted earlier, the complete enclosure of the model within the sabot, and the partial evacuation of the launch tube, are believed to essentially eliminate heating resulting from item 1. The heating resulting from item 2 can be as high as 100 percent of Q_{aero} when no gas seal is used. The effectiveness of the gas seal in reducing this heating can be ascertained from the repeatability of data from several test shots with various seal designs. The heat lost from the model during the low-speed portion of the flight (when the wall temperature may be greater than the recovery temperature) has been found to be small[12.6].

The model may be heated or cooled by friction and conduction as it passes through the catcher and funnel combination. This can be studied experimentally with models preheated to a known temperature and fired at low speeds into the catcher from a compressed air gun placed inside a temperature-controlled oven. Since the amount of energy stored in the model before launch is known, the overall effect of the catching process on the total heat transfer can be evaluated. Reference 12.6 has reported on the basis of such tests that errors of the order of 10 percent of the aerodynamic heating can be introduced in the catcher. This small error, once defined, can be reconciled.

The sum of the estimated errors due to items 1 through 4, in the total heat input measurements of Q_{aero} reported in Reference 12.6, are listed below for three different velocities. As expected, the percentage error diminishes as the launch velocity, and hence, Q_{aero}, increases.

Launch velocity (km/sec)	*Error range (percent)*
1.7	+13 −15
2.3	+ 8 −10
3.3	+ 6 − 8

Because of the method of data reduction used, it is difficult to estimate the accuracy of the heating rates, $\dot{q}_{av}$. The maximum expected error could be larger than the maximum error in the total heat-transfer measurements. As can be seen from Figure 12.12, the difference between the heating rates obtained from the present technique and from well-established theory, for the case of a hemisphere, is near the maximum estimated error in the total heating measurements. However, a part of the disagreement is due to base heating, and as such, should not be classified as measurement error. Thus, it appears that the technique is accurate to the order of 10 percent under the conditions described. This is comparable to the accuracy of more conventional heat-transfer-measurement techniques.

The technique is applicable to determination of heat transfer in gases other than air. Measurement of heat absorbed by ablating bodies can be used to evaluate transpiration blockage effects. Local heating to selected model regions can in principle be measured on segmented models which come apart on entering the catcher if mechanical devices can be designed to allow only the part of interest to enter the calorimeter. Thus, for example, if the blunt tip of a conical model is separated from the parent body by deceleration loads in penetrating the paper sheets, and if a proper sized screen is placed over the calorimeter entrance, only the tip enters the calorimeter, and tip heating is measured.

As noted earlier, the velocity limit of this technique may be imposed by the begining of melting in the stagnation region. This limitation to the catcher-calorimeter technique becomes the basis for the melting-onset technique.

12.5 MELTING-ONSET TECHNIQUE

This technique uses the time of onset of melting in the stagnation region of small metal models as a measure of the stagnation-point heating rate[12.2,12.11]. A sabot-held model is gun-launched at high velocity into either still air or an oncoming airstream. Heating is experienced by the model as it decelerates. This heating serves to raise the temperature of the model and, if heating is prolonged, at some point along its flightpath the surface of the model will begin to melt. Melting occurs first in the stagnation region, where the heating rate is highest. Since the viscosity of the metal used (aluminum) is low, the metal flows off the model surface and into the wake. This liquid aluminum runoff produces a partially opaque screen which is visible in the wake region in spark shadowgraphs. If the free-stream density and model size are adjusted correctly, melting can be made to begin during the portion of the model flight through the instrumented test section of the range; thus, the time at which melting first occurs can be determined from successive shadowgraphs. With the time of melting-onset known, the stagnation-point heating rate can be determined by solving the heat-conduction equation for the model interior. This technique is described in detail in the following sections.

12.5.1 Analysis

In order to relate the melting-onset time to the heat-transfer rate, it is necessary to solve the heat-conduction equation for the interior of the model. Calculations have shown that for the short flight times typical of small ballistic ranges (a few milliseconds) the appreciably heated layer within the model is thin (less than 10 percent of the model diameter), and that the one-dimensional form of the heat-conduction equation can be used. The boundary conditions are those for a semi-infinite slab, initially at uniform temperature, heated on its exposed surface with a time-dependent heating rate. The time dependence of the heating rate arises because of the changing free-stream conditions and velocity along the flightpath.

The equations to be solved are

$$\left.\begin{aligned} a\frac{\partial^2 T}{\partial y^2} &= \frac{\partial T}{\partial t}, \quad y > 0, \quad t > 0 \\ T(y,0) &= T_i \\ -K\left(\frac{\partial T}{\partial y}\right)_{y=0} &= \dot{q}_{st} = \dot{q}_{st}(t), \end{aligned}\right\} \tag{12.16}$$

where T is the temperature, t is time, y is distance into the model surface, K is thermal conductivity, a is thermal diffusivity, and $\dot{q}_{st}$ is the heat-transfer rate at the stagnation point.

The solution of this system is well known and can be written with the aid of Duhamel's integral[12,9]. The surface temperature, T_w, is given by

$$T_w - T_i = \left(\frac{a}{\pi}\right)^{\frac{1}{2}} \frac{1}{K} \int_0^t \dot{q}(t-\tau)\, \frac{d\tau}{\tau^{\frac{1}{2}}}. \tag{12.17}$$

Thus if the heating rate is known as a function of time, the surface-temperature variation with time may be calculated. Under the assumption of constant free-stream density (e.g., when the model is flown into still air) and constant drag coefficient, one form of the trajectory equation is

$$V = \frac{1}{(\rho_\infty A C_D/2m)t + \frac{1}{V_L}}. \tag{12.18}$$

Since the velocity does not change greatly over the trajectory under conditions chosen for this kind of test, the stagnation-point heating rate may be approximated by a less general form of Equation (12.8)

$$\dot{q}_{st} = \gamma V^3, \tag{12.19}$$

where γ depends on ρ_∞ and the body size.

If Equations (12.17), (12.18), and (12.19) are combined, the equation for surface temperature may be written

$$T_w - T_i = \frac{\dot{q}_{st_L}}{K V_L^3}\left(\frac{a}{\pi}\right)^{\frac{1}{2}} \int_0^t \frac{d\tau}{\left[(\rho_\infty A C_D/2m)(t-\tau) + \frac{1}{V_L}\right]^3 \tau^{\frac{1}{2}}}, \tag{12.20}$$

where $\dot{q}_{st_L}$ is the heating rate at the beginning of flight. This may be integrated to give

$$\begin{aligned} T_w - T_i &= \frac{2\dot{q}_{st_L}}{K}\left(\frac{at}{\pi}\right)^{\frac{1}{2}} \left\{ \frac{d^3}{8(bt+d)^2}\left[\frac{2(bt+d)+3d}{d^2} + \frac{3}{2\sqrt{[bt(bt+d)]}} \log_e\left[\frac{\sqrt{(bt+d)}+\sqrt{(bt)}}{\sqrt{(bt+d)}-\sqrt{(bt)}}\right]\right]\right\} \\ &= \frac{2\dot{q}_{st_L}}{K}\left(\frac{at}{\pi}\right)^{\frac{1}{2}} \beta \end{aligned} \tag{12.21}$$

where

$$b = \frac{\rho_\infty A C_D}{2m}, \quad d = \frac{1}{V_L}, \tag{12.22}$$

and β is the term in braces $\{\}$. Equation (12.21) is a closed-form solution for the time dependence of the stagnation-point surface temperature for models fired into still air.

When models are fired through the tunnel-starting-transient flow into a counterflow airstream, it is no longer possible to obtain a closed-form solution and Equation (12.17) must be integrated numerically. The integral is improper at its lower limit and thus unsuitable for numerical integration. A slight alteration of this equation removes the singularity to give

$$T_w - T_i = 2\left(\frac{a}{\pi}\right)^{\frac{1}{2}} \frac{1}{K} \int_0^{\sqrt{t}} \dot{q}_{st}(t-\tau)\, d(\sqrt{\tau}) \quad . \tag{12.23}$$

The numerical integration of Equation (12.23) is best performed on a computer. Equation (12.23) will allow the surface temperature to be computed as a function of time for counterflow airstream operation if the heating rates along the flightpath are known. Reference 12.2 should be consulted for details of this procedure.

12.5.2 Facilities and Test Equipment

No special equipment is required for this experiment. The model (material and geometry) and the test conditions must be selected such that melting occurs in the instrumented test section of the facility which is required to be equipped with shadowgraph stations.

A simple design criterion for estimating these conditions can be obtained on the basis of a constant velocity flight (i.e., constant heat-transfer rate). If $\beta = 1$, the model surface-temperature rise is given from Equation (12.21) as

$$T_w - T_i = \frac{2\dot{q}_{st}}{K}\left(\frac{at}{\pi}\right)^{\frac{1}{2}} \quad . \tag{12.24}$$

Solving for the time to reach melting temperature, setting $x = Vt$ where V is the constant velocity, and using Equation (12.19) gives

$$x_{melt} = \frac{\pi}{a}\left(\frac{[T_{melt} - T_i]K}{2\gamma}\right)^2 \frac{1}{V^5} \quad , \tag{12.25}$$

where x_{melt} is the approximate distance from the gun at which melting begins.

Equation (12.25) allows one to choose the model material, size, and free-stream density for a particular size facility and launch velocity. For example, a 0.635-cm-diameter aluminum hemisphere launched at 7.4 km/sec into air at a free-stream pressure of 70 torr begins to melt in about 7 meters of travel.

12.5.3 Typical Results

The shadowgraphs[12.11] shown in Figure 12.13 illustrate the evidence of melting onset. The model is an aluminum hemisphere 0.635 cm in diameter launched at 7.4 km/sec into air at 70 torr. Six data stations are shown with the corresponding temperatures calculated with Equation (12.21) and the heat-transfer rates of Reference 12.10. No melting is noted in stations one and two, but in station three there is a line of molten material seen coming off the rear of the model. The temperature of the stagnation point is calculated to be 921°K. This is in good agreement with the known melting point of aluminum (7075-T6), which is 911°K. Results from several tests of this type are shown plotted in Figure 12.14. Shown here is the actual observed time to melting onset (abscissa) compared with the theoretical computed time (ordinate). The bar length indicates error bands of the observations. The agreement is very good. A summary of results collected using this technique is shown in Figure 12.15. The shaded area represents some of the available shock-tube data[12.10,12.12,12.13].

12.5.4 Error Considerations

As with all heat-transfer techniques, sources of error in this technique are difficult to evaluate completely. If the results in Figure 12.14 are considered, the deviation of the heating rate from the average is +9 and −13 percent. Part of this can be accounted for by the fact that the model is observed only at discrete times along the flightpath, and therefore, melting onset is always observed sometime after it might first have been observed. On the average this error is −6 percent for the particular test facility used to obtain these results (1.2-meter intervals between stations and approximately 7 meters from gun muzzle to melting onset. Therefore, other sources of error, such as changes in heating during launch, changes in sabot separation from run to run, and angle of attack must account for the remainder of the scatter in these results.

12.5.5 Remarks

This technique, which measures local heating rates, is relatively simple to use and has been used at velocities in excess of earth-escape velocity. Testing times are of the order of 10 to 100 times longer than in shock tubes at the higher speeds. There are, however, sources of error, particularly when the countercurrent airstream is used, which are difficult to assess. In general, the accuracy of the technique can be considered acceptable but not extraordinary. Its principal virtue is that by being different from techniques used in other types of laboratory facilities, it offers an independent method for obtaining experimental data.

Possible applications of the technique are the measurement of heat transfer in planetary gases, the study of the effects of surface catalysis on heat transfer, and, by the provision of low-melting-temperature alloy inserts, the measurement of heat-transfer rates to other parts of the model.

12.6 STUDIES OF SURFACE ABLATION ON RECOVERED MODELS

12.6.1 Model-Recovery Techniques

The techniques of recovering the models used in the catcher-calorimeter tests[12.6] have been applied to plastic models which have suffered moderate ablation as well. The surfaces of the recovered models reveal the extent of the ablation as well as the nature of the flow processes responsible for the ablation, provided that negligible damage is done by the recovery. The first quantitative studies of this kind were done using the paper-arresting device described in Section 12.4.2.2, but only mass-loss data were obtainable since the surface features on the models were removed by passage through the paper sheets. Far superior results were subsequently obtained by simply allowing the model to come almost to rest under aerodynamic deceleration alone[12.14-12.17].

12.6.2 Range Requirements

A plastic model that has decelerated to low speed will frequently stray erratically far from boresight. It is desirable therefore to install a large open-ended tube in the range to guide the model during the last part of its flight to the backstop. The tube aids in model recovery and prevents damage from impacts of the model with down-range shadowgraph stations. Although the model can slide or ricochet along the tube, the damage thus incurred is usually minor and the terminal collision can be postponed until the velocity is reduced sufficiently that the model can impact the backstop without further damage.

Although all of the recovered models from aeroballistic ranges have been fired horizontally and recovered inside airtight enclosures, it seems attractive to consider firing small-scale models vertically in the open air and recovering them after they fall to the ground. This procedure would allow the use of heavier and/or more slender models which will not decelerate sufficiently to be recovered intact within the length of the ballistic range. In a sense this technique is being used in long exterior guided-missile test ranges, where recovery of entry bodies has been effected.

12.6.3 Experimental Requirements

The most critical ballistic requirement for these tests is that the model surface not be marred after preparation for the test. Aside from obvious precautions in handling, this requires great care in the design and construction of sabots to insure that no propellant gas penetrates along the parting surfaces to erode the test surfaces. A sabot used for this type of testing is illustrated in Figure 3.34. It has been found possible to prevent gas leakage by use of a thin obturation cup at the sabot base or by use of thin films of polyester plastic inside the sabot.

During the acceleration in the launch tube the hydrostatic pressure in the model-sabot assembly greatly exceeds the normal working stress for these materials. Voids along the parting surfaces of the sabot fingers near the plastic model can result in permanent deformation of the model surface. When such voids do exist, the damage done so roughens the model that the flight results lose much of their meaning. An alternative design eliminates the fingers, and thus the joints, by use of a one-piece paraffin wax casting covering the front of the model. In addition to aligning the model inside the launch tube, the wax can be matched in density to that of the plastic model reducing the possibility of model failure. On launching, the wax separates from the model quickly because of its low melting point. It is necessary to use a rigid pusher plug behind the wax-encapsulated model.

A somewhat less obvious requirement on the sabot is that all of it separate quickly from the model after emergence from the gun. If even a small part flies along in the near wake, the model base drag will be decreased and the total mass effectively increased. The resulting reduced deceleration leads to excessive ablation, and the occasional collisions will disturb the natural oscillations of the test body.

12.6.4 Experimental Observations

The quantitative studies of the changes wrought by ablation of these models include:

(a) Total mass removal

(b) Local mass removal

(c) Percent of surface covered by triangular areas of transitional and turbulent boundary-layer flow

(d) Stagnation-point mass removal and change of radius of curvature

(e) Identification of tracks of longitudinal vortices in the boundary layer

(f) Discovery of spatially fixed excessive-heating patterns

The first four items are of direct interest to the designer of heat-protection systems, because they document the actual performance of real ablating surfaces under realistic flows. The last two appear to give clues which may lead to far better understanding of important, somewhat orderly, processes in both laminar and turbulent boundary-layer flows over ablating bodies.

The interpretation of measured total mass loss is highly uncertain except for tests in which it is quite clear that the boundary-layer flow was either all laminar or all turbulent during the high-speed part of the flight.

Where the flow has been turbulent on parts of the surface from time to time, it is particularly desirable to establish a reference axis from which measurements can document the surface recession over the entire body. This has been done for 30^{o} half-angle solid plastic cones having a base diameter of 1 cm by using the base plane and a hole in its center to establish a central axis before the test. By use of this hole and the base plane to position the model, silhouette photographs (e.g., Figure 12.16) can be taken before and after tests with such precision that variations in surface recession can be resolved to ±25 microns.

Figure 12.17 shows surface recession measurements from an acetal (Delrin) plastic cone fired at an initial velocity of 5.3 km/sec. A visual examination of the surface of this particular model disclosed one turbulence wedge (a triangular area with increased mass-loss) similar to that shown in the upper picture of Figure 12.18. The surface-recession measurements in Figure 12.17 are for a cone generator (ray) along the center of this wedge, and for two other rays 10^{o} and 180^{o} away from the wedge. Predicted surface-recession profiles for continuously laminar and turbulent flow are also shown for comparison with the measurements. All the measurements indicate laminar flow near the nose of the model. The measurements along the wedge show transition to turbulent flow within the wedge. The measurements along the 10^{o} ray show transition after this generator enters the wedge, while the measurements along the 180^{o} ray indicate nearly laminar flow. These comparisons show that useful interpretations can be made from measurements of local mass-loss.

On a recovered model the sculpture produced by the airflow is sometimes remarkably detailed and reveals features some of which clearly define characteristics of the overlying boundary-layer flow, such as longitudinal vortices and areas of turbulent flow resulting from roughness. In cases where the sculpturing tends to preserve or accentuate the flow features responsible, the end result is also available for study. Figures 12.18 and 12.19 are photographs of these features. Their quantitative interpretation is not completely understood but early efforts are detailed in References 12.14 through 12.17.

If high resolution photographs can be taken while the model is still in high speed flight, it should be possible to relate the profile changes and sculpture to the flow conditions and history with greater confidence. Furthermore, if it is unnecessary to recover the model without damage, it should be possible to study the profiles and surfaces of slender models, which would not otherwise decelerate sufficiently, and to study the phenomena over broader ranges of Reynolds number.

The detailed study of shadowgraphs and laser photographs for measurement of profile changes has been attempted[12.18,12.19]. Serious attempts to observe the sculpturing process during flight have not yet been made, but the possibility does not seem remote. Figure 12.20 is a reflected-light laser photograph of a slender bimetal cone in flight at a velocity of 3.9 km/sec. The resolution of detail in the metal surface features, the clarity of the bimetal joint, and the sharpness of the profile demonstrate that the state-of-the-art required for such real-time photography is probably in hand.

REFERENCES

12.1 Yee, Layton. Bailey, Harry E. Woodward, Henry T. — *Ballistic-Range Measurements of Stagnation-Point Heat Transfer in Air and in Carbon Dioxide at Velocities up to 18,000 feet per second.* NASA TN D-777, 1961.

12.2 Compton, Dale L. Chapman, Gary T. — *Two New Free-Flight Methods for Obtaining Convective-Heat-Transfer Data.* AIAA Aerodynamic Testing Conference, Washington, DC, March 9-10, 1964.

12.3 Clemens, Paul L. — *Bibliography: Radio Telemetry to Survive High Accelerations.* AEDC-TDR-63-36, February 1963.

12.4 Terman, Frederick Emmons — *Radio Engineering.* 2nd edition. McGraw-Hill, 1937.

12.5 Chapman, Dean R. — *An Approximate Analytical Method for Studying Entry Into Planetary Atmospheres.* NACA TN 4276, 1958.

12.6 Chapman, Gary T. Jackson, Charles T. Jr — *Measurement of the Heat Transfer to Bodies of Rdvolution in Free-Flight by Use of a Catcher Calorimeter.* NASA TN D-1890, 1963.

12.7 Fay, J.A. Riddell, F.R. — *Theory of Stagnation Point Heat Transfer in Dissociated Air.* J. Aero. Science, Vol.25, No.2, February 1958, pp.73-85.

12.8 Stine, Howard A. Wanlass, Kent — *Theoretical and Experimental Investigation of Aerodynamic-Heating and Isothermal Heat-Transfer Parameters on a Hemispherical Nose With Laminar Boundary Layer at Supersonic Mach Numbers.* NACA TN 3344, 1954.

12.9 Carslaw, H.S. Jaeger, J.C. — *Conduction of Heat in Solids.* 2nd edition. Oxford University Press, London, 1959.

12.10 Hoshizaki, H. — *Heat Transfer in Planetary Atmospheres at Super-Satellite Speeds.* ARS J., Vol.32, No.10, October 1962, pp.1544-51.

12.11 Compton, Dale L. Cooper, David M. — *Free-Flight Measurements of Stagnation-Point Convective Heat Transfer at Velocities to 41,000 ft/sec.* NASA TN D-2871, June 1965.

12.12 Rose, P.H. Stankevics, J.O. — *Stagnation Point Heat Transfer Measurements in Partially Ionized Air.* Res. Rep. 143, Avco-Everett Res. Lab., April 1963.

12.13 Offenhartz, E. Weisblatt H. Flagg, R.F. — *Stagnation Point Heat Transfer Measurements at Super-Satellite Speeds.* J. of Royal Aero. Soc., Vol.66, No.613, January 1962, p.54.

12.14 Wilkins, Max E. — *Evidence of Surface Waves and Spreading of Turbulence on Ablating Models.* Tech. Note, AIAA J., Vol.3, No.10, October 1965, pp.1963-1966.

12.15 Wilkins, Max E. Tauber, Michael E. — *Boundary-Layer Transition on Ablating Cones at Speeds up to 7 km/sec.* AIAA J., Vol.4, No.8, August 1966, pp.1344-1348.

12.16 Canning, Thomas N. Wilkins, Max E. Tauber, Michael E. — *Boundary-Layer Phenomena Observed on the Ablated Surfaces of Cones Recovered After Flights at Speeds up to 7 km/sec.* AGARD Specialists' Meeting on Fluid Physics of Hypersonic Wakes, Colorado State Univ., Fort Collins, Colorado, May 10-12, 1967.

12.17 Canning, Thomas N. Wilkins, Max E. Tauber, Michael E. — *Ablation Patterns on Cones Having Laminar and Turbulent Flows.* AIAA J. Tech. Note, AIAA J., Vol.6, No.1, January 1968, pp.174-175.

12.18 Palkin, S.N. Reznikov, B.I. Studenkov, A.M. Bykov, V.N. — *Investigation of the Ablation of Low-Melting-Temperature Models on a Ballistic Facility.* (Issledovanie unosa massy legkoplavkikh modelei na ballisticheskoi ustanovke). In book "Aerophysical Studies of Supersonic Flows". (Aerofizicheskie Issledovaniia Sverkhzvukovykh-Techenii) ed. Iu. A. Dunaev. Moscov, Isdatel'stvo Nauka, 1967.

12.19 Collins, D.J. Rogers, W.K. Sangster, D.K. — *Microsphere Ablation in a Free-Flight Range.* AIAA J., Vol.5, September 1967, pp.1684-1685.

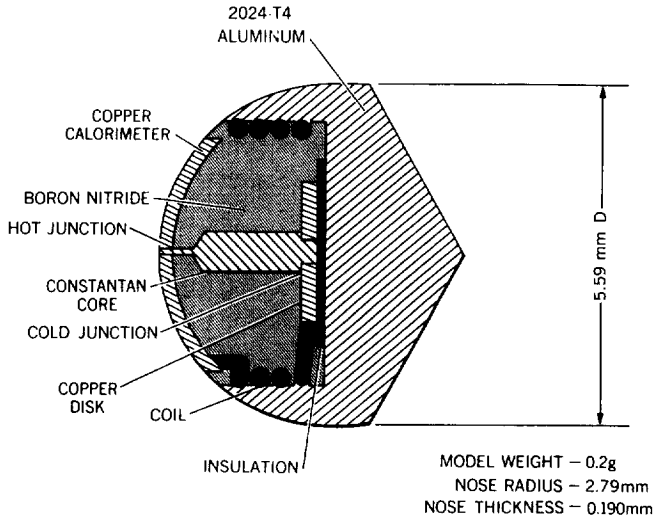

Fig. 12.1 Thermocouple model

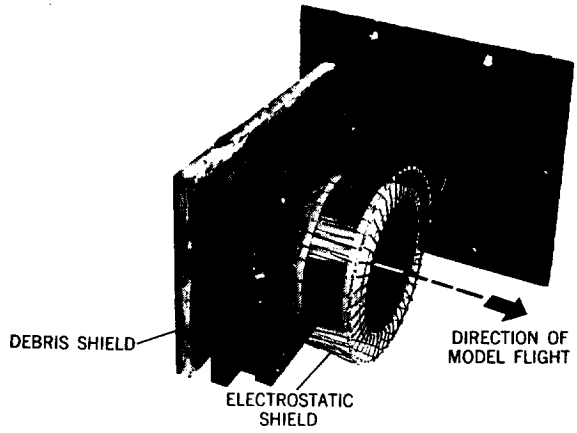

Fig. 12.2 Pickup-coil assembly; coil diameter = 10 cm

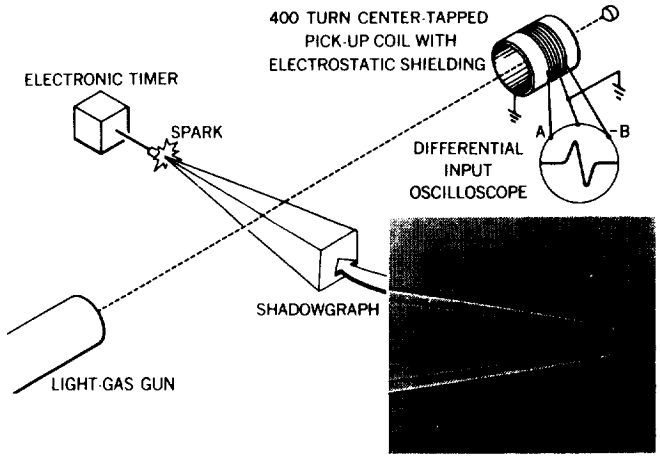

Fig. 12.3 Experimental setup

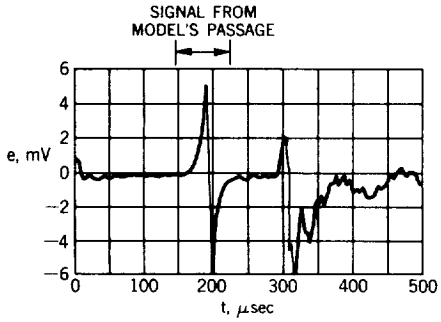

Fig. 12.4 Oscillogram of signal

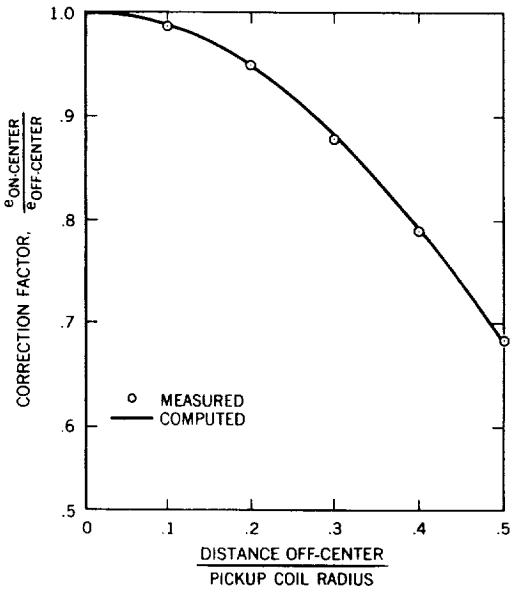

Fig. 12.5 Correction for off-center shot $\left(\frac{\text{Pickup coil R}}{\text{Model coil R}} = 23.5\right)$

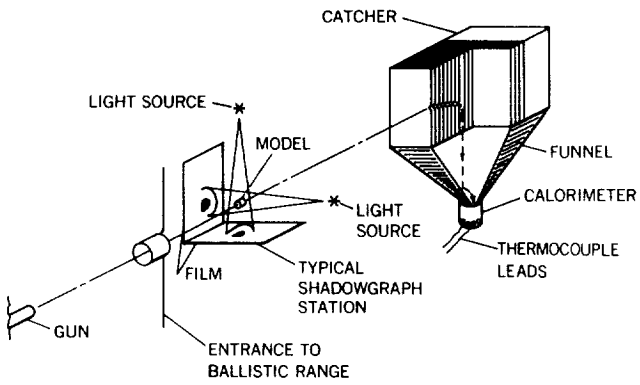

Fig. 12.6 Schematic drawing of test setup

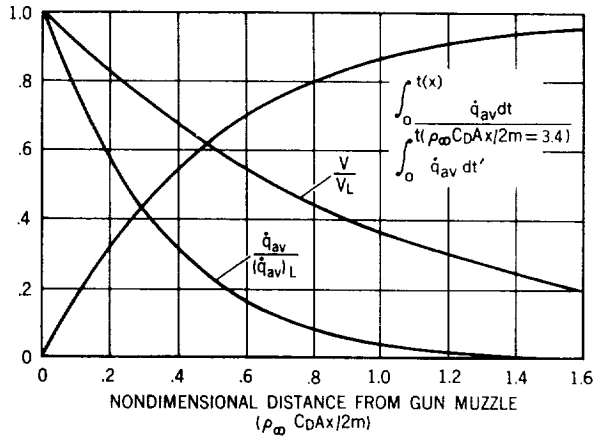

Fig. 12.7 Variations in heating and velocity with distance from the gun

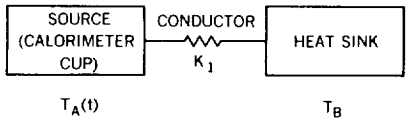

Fig. 12.8 Block diagram of calorimeter

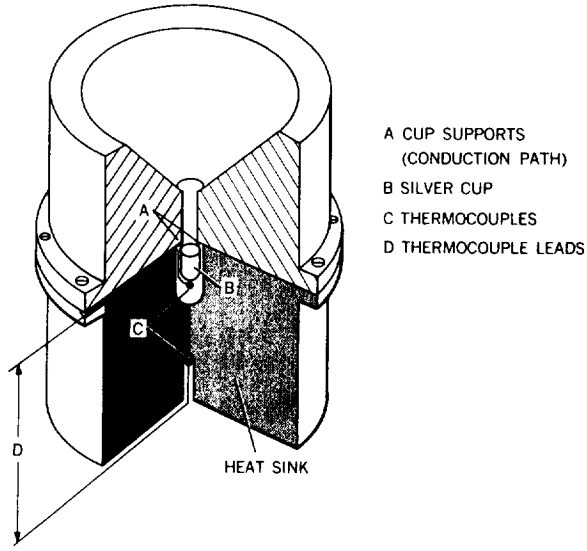

Fig. 12.9 Quarter-sectional drawing of the calorimeter

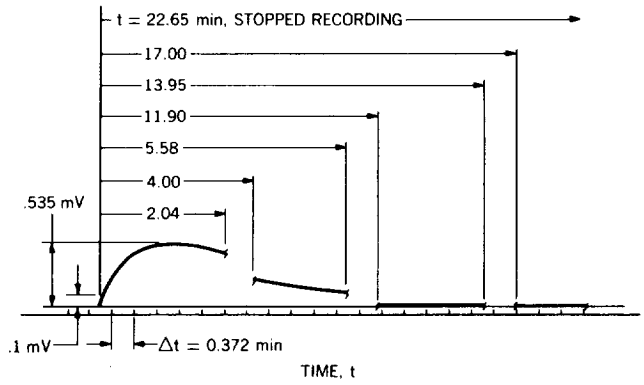

Fig. 12.10 Typical calorimeter output trace

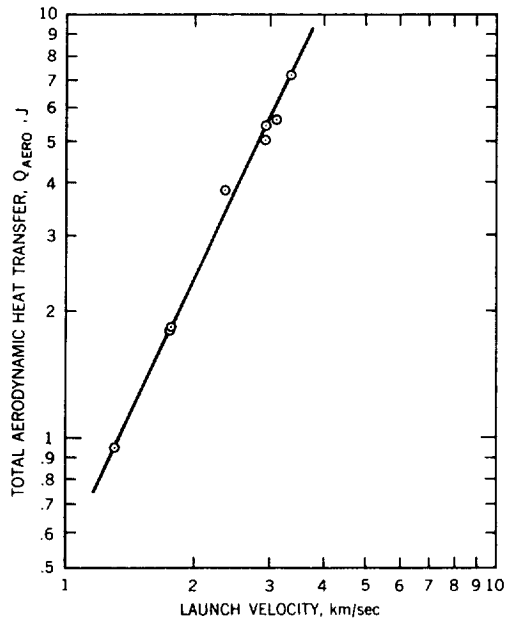

Fig. 12.11 Heat transfer to a 0.635-cm-diameter hemisphere at 1-atmosphere free-stream pressure

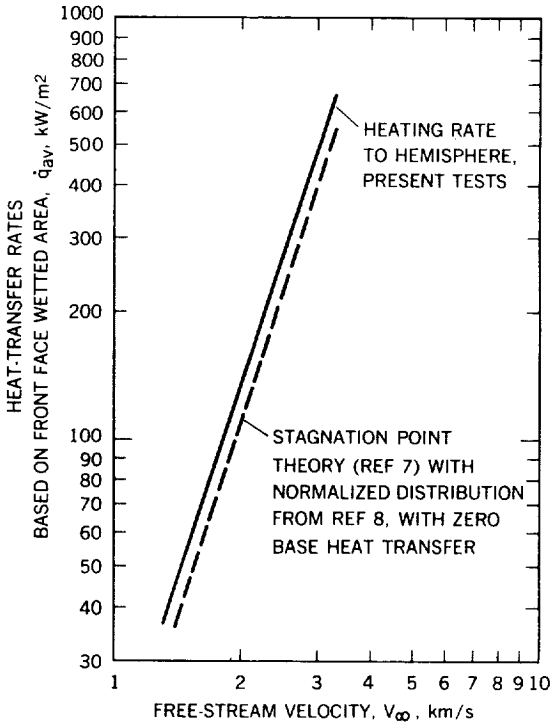

Fig. 12.12 Comparison of the experimental and theoretical heat-transfer rates, based on front-face wetted area, for a 0.635-cm-diameter hemisphere

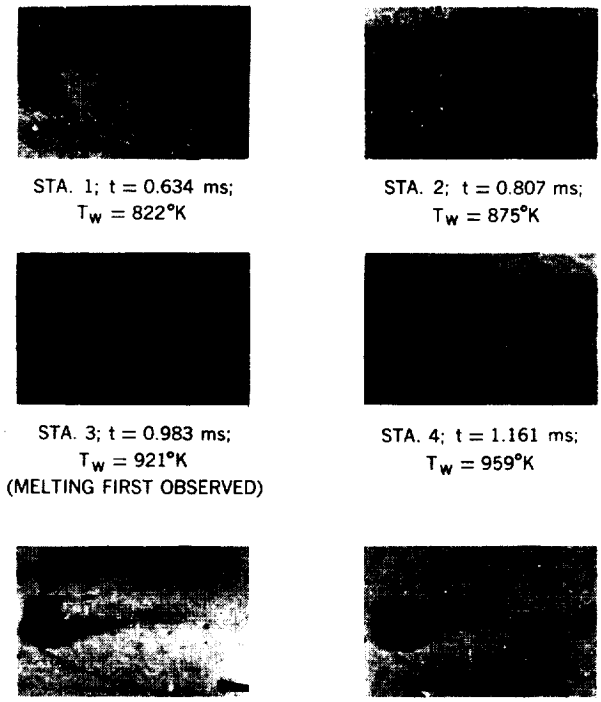

Fig. 12.13 Shadowgraphs showing onset of melting

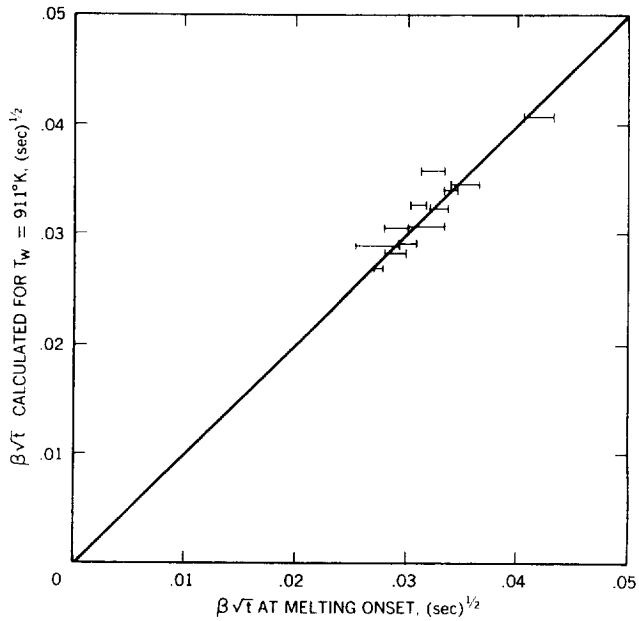

Fig. 12.14 Correlation plot for 7.3 km/sec data

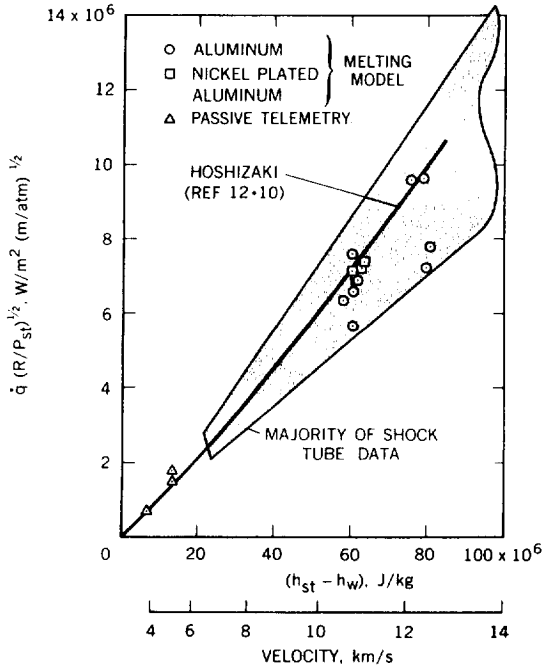

Fig. 12.15 Summary of results; h_{st} = stagnation enthalpy, h_w = wall enthalpy, R = nose radius, P_{st} = stagnation pressure

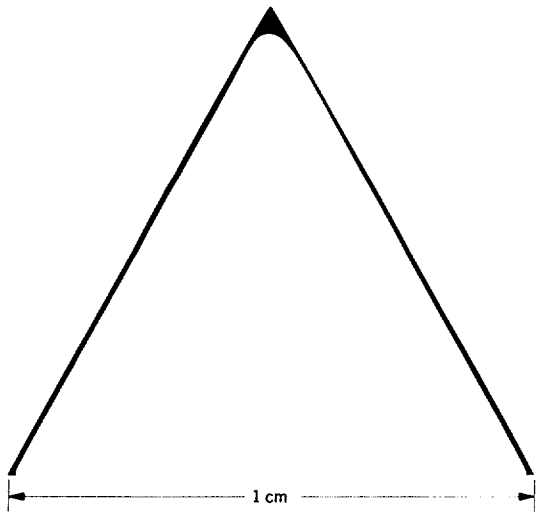

Fig. 12.16 Before and after silhouettes of Delrin (acetal) model; launch velocity, 6.4 km/sec

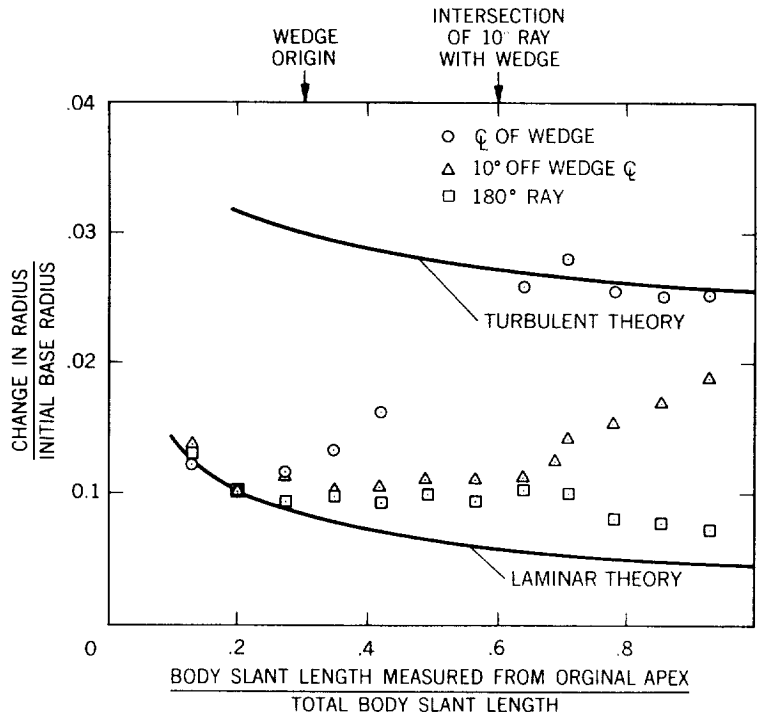

Fig. 12.17 Surface recession profiles of a 30° half-angle conical Delrin model with turbulence wedges. Launch velocity, 5.3 km/sec; mass loss, 3.80%; slant-length Reynolds number based on boundary-layer-edge properties at launch, 5.3×10^{6}; range pressure, 1 atm air

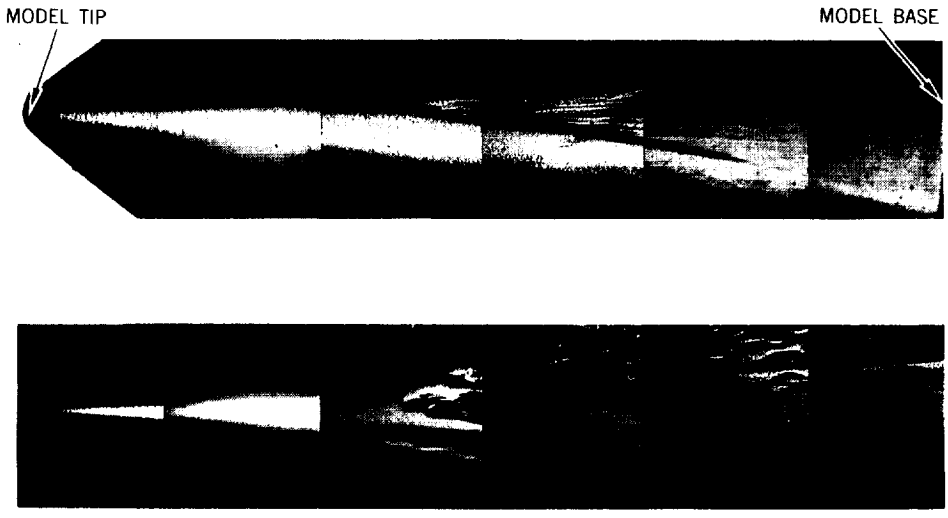

Fig. 12.18 Photomicrographs of surfaces of recovered Lexan (polycarbonate) models

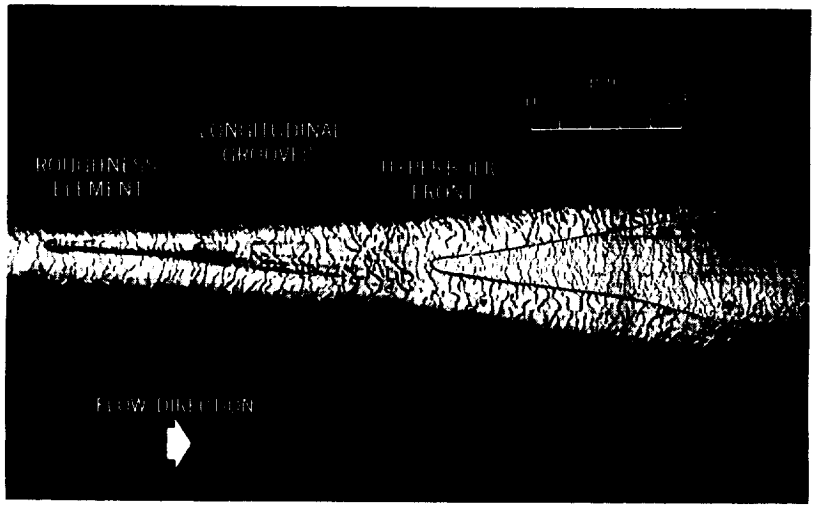

Fig. 12.19 Turbulence wedge on recovered Lexan model

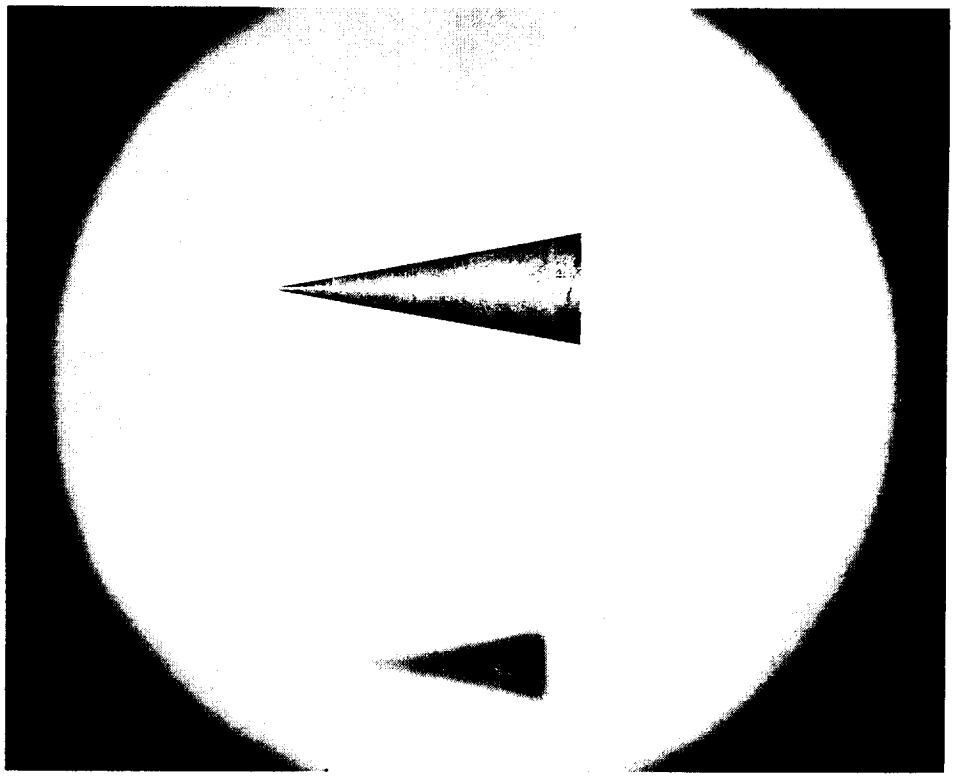

Fig. 12.20 Reflected-light photograph of a 10-degree semi-angle cone in the VKF 1000-ft Hypervelocity Range, exposed with a 20-nsec laser pulse. Model is constructed with a copper nose and aluminum afterbody. Base diameter = 25.4 mm; velocity = 3.9 km/sec; range press. = 49 mm Hg. (Courtesy of von Kármán Gas Dynamics Facility, Arnold Engineering Development Center.)